Interactive Visualizations of Blowups of the Plane

Peter Schenzel and Christian Stussak

Abstract—Blowups are an important technique in algebraic geometry that permit the smoothing of singular algebraic varieties. It is a challenge to visualize this process even in the case of blowups of points X in the affine plane $\mathbb{A}^2_{\mathbb{R}}$. First results were obtained by Brodmann with the aid of the so-called toroidal blowup, a compact embedding of the blowup into affine 3-space. In fact, Brodmann provides a rational parametrization of the toroidal blowup, but its visualization fails in the neighborhood of X because the parametrization tends to indefinite terms of the form $\frac{0}{0}$. Our approach is based on implicitization of the parametric form. By methods from commutative algebra we are able to reduce the implicitization to the computation of a single, fairly simple resultant. This provides an algebraic equation of the implicit surface of the toroidal blowup including the so-called exceptional fiber associated with X. Surprisingly, the degree of the equation grows only linearly with the degree of the parametrization. By applying additional clipping techniques to the implicit surface we are able to visualize the toroidal blowup as well as its deformations by several parameters interactively in real time using GPU-based ray casting techniques. The methods of the paper provide insights in the structure of blowups of points, even if the points are interactively moved or tend to degenerations.

Index Terms—Toroidal blowup, implicitization, real-time ray tracing, interactive surface deformation

1 Introduction

We start with an example to motivate the vizualization of blowups of the plane. Consider the cubic plane curve defined as the zero set of the polynomial $C = u^2 - v^2(v+1) \in \mathbb{R}[u,v]$ shown in red on the lower left of Fig. 1. This curve has a well-defined tangent at all points except for the origin $(0,0)$, where two lines are tangent to C. This point of the curve is called singular. In general, it is much easier to understand the properties of an algebraic variety (e.g., an algebraic curve), if it is nonsingular.

In order to smooth the singularities of an algebraic variety, blowups are an essential technique [1], [2]. By replacing the singularities of any complex algebraic variety V by an appropriately chosen sequence of blowups, one eventually obtains a nonsingular variety $\tilde{V}$. That this process finishes with a nonsingular model was proved by Hironaka (see [1]).

We illustrate this concept using again the curve C, restricted to a disc

$$\mathbb{D} = \{(u,v) \in \mathbb{A}^2_{\mathbb{R}} | u^2 + v^2 \leq \rho^2\}, \tag{1}$$

of radius ρ as reproduced in the lower part of Fig. 1. This restriction has some advantages for the visualization as we will see later on. In order to blow up the disc $\mathbb{D}$ in the origin we first move over to the affine 3-space by mapping a given point $(u,v) \in \mathbb{D}$, $v \neq 0$, to $(u,v,\frac{u}{v}) \in \mathbb{R}^3$.

This yields a parametrization of a surface $\mathbb{S}_0$ over the disc excluding the line $v = 0$. The vertical line through the origin becomes part of the topological closure of $\mathbb{S}_0$. The resulting closed surface $\mathbb{S}$ is shown in the upper left part of Fig. 1.

Now, we apply the mapping $(u,v) \mapsto (u,v,\frac{u}{v})$ to $(\mathbb{D} \setminus V(v)) \cap V(C)$, i.e., we lift the plane curve C onto $\mathbb{S}_0$. The closure of the resulting space curve (illustrated in red color in the top left in Fig. 1) is nonsingular.

The construction excludes all the points on the v axis since we cannot divide by zero. Therefore, we may swap the roles of u and v and repeat the process by mapping $(u,v) \in \mathbb{D}$, $u \neq 0$ to $(u,v,\frac{v}{u})$ obtaining the surfaces $\tilde{\mathbb{S}}_0$ and $\tilde{\mathbb{S}}$. Mathematically, it is more convenient to work with only one surface $\mathbb{B}$ in $\mathbb{A}^2_{\mathbb{R}} \times \mathbb{P}$ (using the projective instead of the real line) given by the closure of $\mu(\mathbb{D} \setminus \{(0,0)\})$, $\mu : (u,v) \mapsto (u,v,(u:v))$. We call $\mathbb{B}$ the *blowup* of the disc in the origin and $\mathbb{S}$ and $\tilde{\mathbb{S}}$ are called the *two affine charts* of $\mathbb{B}$. Since we blow up the disc based on the rational map $(u,v) \mapsto (u:v)$ we use the more precise notation $\mathbb{B}_{u,v}$, where appropriate.

In order to visualize the surface $\mathbb{B}$ we could visualize its two affine charts. But this is not a satisfying solutions since both, $\mathbb{S}$ and $\tilde{\mathbb{S}}$, are infinite surfaces. Only a small part of the geometry is visualizable in a finite viewport. A nice approach is to use an appropriate embedding of $\mathbb{B}$ into 3-space, such as the one utilized in [3] (see also [4] for a full length treatment in German). That is, a certain type of a stereographic projection is used in order to transform the projective lines over each point of $\mathbb{D}$ into circles. Therefore, the infinite solid cylinder over $\mathbb{D}$ is mapped into a solid torus. Applying this transformation to $\mathbb{B}$ yields a compact model $\mathbb{T}$ of $\mathbb{B}$ in 3-space. We call the surface $\mathbb{T}$ the *toroidal blowup*. In our concrete example, the chart $\mathbb{S}_{u,v}$ of $\mathbb{B}_{u,v}$ is transformed into the so-called Möbius strip as shown on the right side of Fig. 1. Note that the curve C is transformed into a nonsingular curve onto the Möbius strip.

The generators $u = 0, v = 0$ are a good choice in order to obtain an appropriate blowup of the disc in the origin that

• *The authors are with the Institute of Computer Science, Martin-Luther-University, Halle-Wittenberg, D-06099 Halle, Germany. E-mail: {schenzel, stussak}@informatik.uni-halle.de.*

Manuscript received 19 Dec. 2011; revised 9 May 2012; accepted 4 July 2012; published online 10 July 2012.
Recommended for acceptance by D. Weiskopf.
For information on obtaining reprints of this article, please send e-mail to: tvcg@computer.org, and reference IEEECS Log Number TVCG-2011-12-0315.
Digital Object Identifier no. 10.1109/TVCG.2012.161.

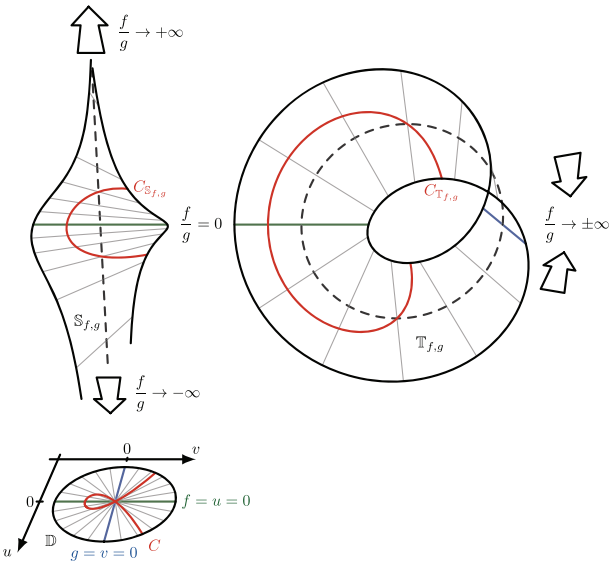

Fig. 1. The singular plane curve C in the disc $\mathbb{D}$ (lower left) becomes a smooth space curve when lifted to the blowup $\mathbb{B}_{f,g}$ of $\mathbb{D}$ in the origin given by the intersection of $f = u = 0$ and $g = v = 0$. The first affine chart $\mathbb{S}_{f,g}$ of the surface $\mathbb{B}_{f,g}$ is shown in the upper left. To cover $\mathbb{B}_{f,g}$ completely, another affine chart $\tilde{\mathbb{S}}$ is needed (not shown). Furthermore, $\mathbb{S}_{f,g}$ and $\mathbb{S}_{f,g}$ are infinite surfaces, so that most of their geometry can not be visualized directly. The transformation of the infinite cylinder over $\mathbb{D}$ into a torus yields a suitable embedding of the blowup in affine 3-space as shown on the right.

resolves the singularities of C. But plane curves with several or more complicated singularities require different generators, e.g., so that the disc is blown up in more than one point. We will investigate the concept of blowups of the disc in a finite number of points defined by the vanishing of two polynomials in the next section.

1.1 The Definition of Blowups

In general, the blowup of the real affine plane in a finite set of points $X = V(f, g) = \{P_1, \ldots, P_r\} \subset \mathbb{A}^2_{\mathbb{R}}$ is obtained as follows: Consider the map

$$\begin{aligned} \mu{:}\mathbb{A}^2_{\mathbb{R}} \setminus X &\to \mathbb{A}^2_{\mathbb{R}} \times \mathbb{P}^1_{\mathbb{R}}, \\ (u, v);\ &\mapsto ((u, v), (f(u, v) : g(u, v))), \end{aligned} \tag{2}$$

where $f, g \in \mathbb{R}[u, v]$ are polynomials with the zero set $X = V(f, g)$. Note that f and g do not have a common factor. Then, the blowup $\mathbb{B}_{f,g}$ of $\mathbb{A}^2_{\mathbb{R}}$ in X is defined as the closure of $\mu(\mathbb{A}^2_{\mathbb{R}} \setminus X)$ in $\mathbb{A}^2_{\mathbb{R}} \times \mathbb{P}^1_{\mathbb{R}}$. There is a natural map π: $\mathbb{B}_{f,g} \to \mathbb{A}^2_{\mathbb{R}}, (u, v, (s : t)) \mapsto (u, v)$. The preimage $\pi^{-1}(X) \subset \mathbb{B}_{f,g}$ is called the *exceptional fiber* $\mathbb{E}$. It consists of the union of projective lines over the points $P_i \in X, i = 1, \ldots, k$. Moreover, π induces an isomorphism $\mathbb{A}^2_{\mathbb{R}} \setminus X \simeq \mathbb{B}_{f,g} \setminus \mathbb{E}$. For further technical details, we refer to a textbook on Algebraic Geometry, e.g., [2] and [5, pp. 506-508].

1.2 The Embedding into a Torus

An interesting question is how a blowup of the plane in a finite number of points $X = V(f, g)$ looks like. As mentioned in the initial example, the embedding of the blowup of the disc $\mathbb{D}$ into affine 3-space by transforming the infinite cylinder over $\mathbb{D}$ into a solid torus is a promising approach.

This idea has been carried out in detail in [4]. The composition of the stereographic projection with a certain

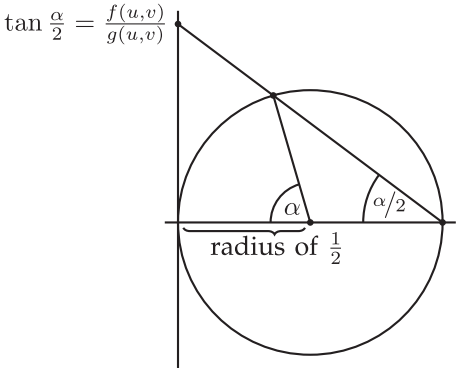

Fig. 2. Computation of the angle α for a point of height $\frac{f(u,v)}{g(u,v)}$ over $\mathbb{D}$ in order to map this point onto a circle as proposed in [4]. Note that α only depends on the height $\frac{f(u,v)}{g(u,v)}$ of the point but not on its (u, v) coordinates in the disc.

diffeomorphism provides the following parametrization $P(u, v)$ of the image of $\mathbb{D} \setminus V(f, g)$ in $\mathbb{D} \times \mathbb{P}^1_{\mathbb{R}}$ embedded as a solid torus with central radius $r \in \mathbb{R}$, $r > \rho$ in $\mathbb{A}^3_{\mathbb{R}}$:

$$(u, v) \mapsto (u, (v - r)\cos\alpha, (r - v)\sin\alpha). \tag{3}$$

Following Fig. 2 the angle α is defined as

$$\alpha = \begin{cases} 2\arctan\frac{f(u,v)}{g(u,v)} & g(u, v) \neq 0, \\ \pi & g(u, v) = 0. \end{cases} \tag{4}$$

This can be simplified by applying the double angle formulas of sine and cosine to (3). It yields a rational parametrization $P(u, v) = (x, y, z) \in \mathbb{A}^3_{\mathbb{R}}$ with

$$\begin{aligned} x &= u, \\ y &= (r - v)\frac{f^2 - g^2}{f^2 + g^2}, \\ z &= (r - v)\frac{2fg}{f^2 + g^2}. \end{aligned} \tag{5}$$

The image of $\mathbb{D} \setminus V(f, g)$ is now contained in the torus with equation $x^2 + (r - \sqrt{y^2 + z^2})^2 = \rho^2$, which we call the $\mathbb{D}$-torus. The set of points we have to visualize is $\mathbb{T}_{f,g}$, the closure of $\{P(u, v) \in \mathbb{A}^3_{\mathbb{R}} : (u, v) \in \mathbb{D} \setminus V(f, g)\}$ (in the Zariski topology). Under the transformation into the torus the exceptional fiber $\mathbb{E}$ is mapped to a family of circles, one circle for each point of $V(f, g)$. Note that in contrast to the original parametrization in [4] we centered the torus at the origin in order to realize additional symmetry.

1.3 On the Drawbacks of the Parametrization

For the case of toroidal blowups of the plane in $X = \{(0, 0)\}$ a few static renderings have been realized in [4]. This includes, for example, the Möbius strip ($f = u, g = v$) and the Whitney double umbrella ($f = u^2, g = v^2$). The case of four points $X = \{(\pm 1, \pm 1)\} = V(u^2 - 1, v^2 - 1)$ is illustrated as an excellent hand drawing (see [4, Figs. 11 and 12]).

The first, naïve idea for the visualization of a parametrically defined surface is to create a triangle mesh based on an appropriate set of parameters $(u_i, v_i) \in \mathbb{D}, i = 1, \ldots, N$. This approach works well for parametrizations of nonsingular surfaces without parametric singularities.

(a) Filled (b) Wireframe (c) Faulty triangles removed

Fig. 3. Rendering of the parametric form of the toroidal blowup using $f = u, g = v$ (Möbius strip) and one million vertices. The triangles generated near $X = V(f,g) = \{(0,0)\}$ span across the torus, thus, pretending a different surface geometry as shown in (a) and (b). Removing all triangles with $\sqrt{u^2+v^2} < \varepsilon$ results in (c).

(a) Filled (b) Wireframe (c) Faulty triangles removed

Fig. 4. The approach of Fig. 3 applied to $f = v^2 - u(u-1)(u+1)$ and $g = v^2$. Many more wrong triangles are generated near $X = V(f,g) = \{(-1,0),(0,0),(1,0)\}$. Additionally, cancelation errors occur during the computation of the normals (colored in black). In this example, removing all wrong triangles as shown in (c) yields large gaps in the visualization. Note that Fig. 10b shows a correct visualization of this surface using our method.

The following problems arise in the case of toroidal blowups of the plane:

- The numerical computation of $P(u,v)$ becomes unstable in the neighborhood of the zero set $V(f,g)$.
- The parametric normal $\vec{n}(u,v) = (\frac{\partial P}{\partial u} \times \frac{\partial P}{\partial v})(u,v)$ necessary for the shading is a rational expression containing f and g in the eighth power. Numerical instabilities frequently occur near $V(f,g)$.
- The constructed triangles might have extremal sizes, e.g., large edges and very small height. Triangles that span a large range of angles in the torus must be avoided. Otherwise holes and visualization artifacts might occur.
- For sufficiently satisfactory images, N needs to be rather large. Moreover, the points (u_i, v_i) have to be chosen very carefully to provide a good approximation of the surface.
- Points $P(u,v)$ close to the exceptional fiber must be appropriately connected with the exceptional fiber above $V(f,g)$.
- For given $f, g \in \mathbb{R}[u,v]$ the zero set $V(f,g)$ is not known a priori. Its computation requires additional effort.
- The triangulation has to be recomputed for any deformation of f and g.

Visualizations of two toroidal blowups based on the parametric form and a uniform subdivision of the parameter space are reproduced in Figs. 3 and 4. This is the approach carried out in [4]. It is easy to see that the visualization of simple toroidal blowups can be achieved by omitting all (u,v) close to $X = V(f,g)$ (Fig. 3). This solution does not extend to more complicated polynomials f and g, which becomes apparent in Fig. 4.

In order to create triangulations of a wider range of toroidal blowups a more sophisticated method has been studied by A. Prager in his diploma thesis [6]. He created high-quality polygonal meshes of toroidal blowups using methods from differential geometry to trace the level curves of the blowup $\mathbb{B}_{f,g}$ over the disc. The surface is formed by connecting the approximations of the level curves while taking special care of the regions close to the exceptional fibers. With this idea he has been able to visualize, for example, the blowup in the four points $X = \{(\pm 1, \pm 1)\}$ mentioned above. The improved visualization is done at the expense of time-consuming precomputations. Therefore, this method is inappropriate for interactive deformations of the generators f and g.

1.4 Implicitization Based Real-Time Visualization

About 20 years of development in the field of Computer Graphics have passed since Brodmann's approach. A big step during the last years was the introduction of the technique of GPU programming. This allows an interactive visualization and parametric deformation of implicit surfaces in real time by ray casting methods (e.g., see the program REALSURF by Stussak [7]). A technical overview and samples of visualizations can be found in [8], [7], [9], [10], [11].

We demonstrate that these are suitable approaches for the visualization of toroidal blowups and its deformations by utilizing an implicit form of the toroidal blowup rather than a parametric one. A major advantage of the implicit form is that the points of the exceptional fiber are part of the surface. In contrast to the parametric form, no special treatment is necessary for these points.

It is well known that an implicit (algebraic) equation $\mathcal{F}$ for any rationally parametrized surface can be derived by elimination techniques. In the case of a toroidal blowup, three variables need to be eliminated from a system of four algebraic equations (see Section 2). This can be accomplished by Gröbner bases methods [5] or multipolynomial resultants [12], [13] and others. Since the polynomials f and g occur quadratically in (5), this suggests a high degree of $\mathcal{F}$ as a result of the elimination process. Therefore, this approach seems to be computationally rather complex at first glance. A closer examination based upon some techniques of commutative algebra surprisingly shows that the elimination can be done by the computation of a single, very simple resultant of two polynomials. Furthermore, we will prove that the result, i.e., the polynomial $\mathcal{F}$, has an unexpected low degree.

Once the implicit form $\mathcal{F}$ has been obtained, we are able to visualize the surface $V(\mathcal{F})$ and its deformation based on the deformation of f and g in real time. Since $\mathbb{T}_{f,g} \subset V(\mathcal{F})$, we present appropriate clipping techniques to display exactly the toroidal blowup $\mathbb{T}_{f,g}$ but not $V(\mathcal{F}) \setminus \mathbb{T}_{f,g}$. Additionally, different texturing schemes are applied to the surface to get a better understanding of the relation between the toroidal blowup and the disc $\mathbb{D}$.

2 Derivation of the Implicit Form

For the impatient reader the mathematical results of this section can be summarized as follows:

- The implicit equation of the toroidal blowup is
$$\mathcal{F} = \mathrm{Res}_v(F,H)/z = \mathrm{Res}_v(G,H)/z = 0, \quad (6)$$
where $F = fz - ((r-v)+y)g$, $G = gz - ((r-v)-y)f$, $H = y^2+z^2-(r-v)^2$, and u is substituted by x in f and g.
- The degree and the time for the computation of $\mathcal{F}$ grow linearly with the degree of f and g and not quadratically as one would expect.
- Parameters of f and g used for the deformation of the blowup occur as parameters of $\mathcal{F}$. The implicit form $\mathcal{F}$ is independent of the order of elimination and the specialization of the parameters as long as f and g intersect in a finite number of points.

Since our results on elimination are valid in a more general context than the field of real numbers, we switch from $\mathbb{R}$ to an arbitrary infinite ordered field K of characteristic $\neq 2$ during the derivation of the above results.

2.1 Algebraic Preparations

The substitution $u = x$ in the polynomials $f(u,v)$ and $g(u,v)$ provides the following parametrization of the toroidal blowup

$$y = (r-v)\frac{f^2-g^2}{f^2+g^2}, z = 2(r-v)\frac{fg}{f^2+g^2}, \quad (7)$$

where now $f, g \in K[x,v]$. Therefore, in order to obtain the implicit equation of the surface we have to eliminate the variable v from the previously given rational parametrization. Consequently, we obtain the implicit equation of the surface by eliminating the variables v, w from the ideal

$$I = \langle A, B, 1 - w(f^2+g^2)\rangle \quad (8)$$

$$A = y - (r-v)w(f^2-g^2) \quad (9)$$

$$B = z - 2(r-v)wfg, \quad (10)$$

in the polynomial ring $K[x,y,z,v,w]$ with $f, g \in K[x,v]$ (see, e.g., [5]). The auxiliary variable w and the equation $1 - w(f^2+g^2) = 0$ allow to work with a system of polynomials instead of rational functions without changing the set of solutions.

Proposition 1. *With the previous notation define*

$$F = fz - ((r-v)+y)g, \quad (11)$$

$$G = gz - ((r-v)-y)f. \quad (12)$$

Then, $I = \langle F, G, 1 - w(f^2+g^2)\rangle$.

Proof. We define $J = \langle F, G, 1 - w(f^2+g^2)\rangle \subset K[x,y,z,v,w]$. We first show that $F, G \in I$, so that $J \subseteq I$. By subtracting $\pm((r-v) - (r-v)w(f^2+g^2)) \in I$ from $A \in I$ it follows that

$$F' = (r-v) - y - 2(r-v)wg^2 \in I, \quad (13)$$

$$G' = (r-v) + y - 2(r-v)wf^2 \in I. \quad (14)$$

Then, $F = Bf - G'g \in I$ and $G = Bg - F'f \in I$, as required.

In order to show $I \subseteq J$ first note that we have $B = w(Ff+Gg) + z(1 - w(f^2+g^2)) \in J$. Second, it follows that $A = -w(Fg - Gf) + y(1 - w(f^2+g^2)) \in J$, which finally completes the proof. □

For the use in Section 2.2 we need an elementary statement about a certain ideal.

Proposition 2. *With the previous notation define the ideal* $J = \langle F, G, H\rangle \subset K[x,y,z,v]$, *where* $H = y^2+z^2-(r-v)^2$.

1. *The ideal J is generated by the 2×2-minors of the matrix*
$$\begin{pmatrix} f & z & (r-v)+y \\ g & (r-v)-y & z \end{pmatrix}. \quad (15)$$
2. *There are the equalities*
$$J \cap \langle (r-v)+y, z\rangle = \langle F, H\rangle, \quad (16)$$
$$J \cap \langle (r-v)-y, z\rangle = \langle G, H\rangle. \quad (17)$$

Proof. The statement 1 is easy to check. For the proof of statement 2 consider the equalities

$$\begin{aligned} J \cap \langle (r-v)+y, z\rangle &= \langle F, H, \langle (r-v)+y, z\rangle \cap \langle G\rangle\rangle \\ &= \langle F, H, \langle (r-v)+y, z\rangle G\rangle. \end{aligned} \quad (18)$$

The last equality follows since $\langle (r-v)+y, z\rangle$ is a prime ideal and $G \notin \langle (r-v)+y, z\rangle$. But now $\langle (r-v)+y, z\rangle G \subset \langle F, H\rangle$, as follows by the trivial relations among the 2×2-minors of the matrix given in statement 1. This proves the first equality. The proof of the second statement follows the same line of arguments. □

2.2 Elimination

In order to find the defining equation of the surface obtained by the toroidal blowup we have to find the elimination ideal of $I \subset K[x,y,z,v,w]$ in $K[x,y,z]$ for given $f, g \in K[x,v]$. Of course this might be done using a computer algebra system, which supports Gröbner basis. Since the worst case complexity of computing a Gröbner basis for a given ideal is double-exponential (in the degree of the generators of the ideal), our main objective is the reduction of computational complexity. Even for polynomials f, g of low degree, a computer algebra system like SINGULAR runs out of memory when eliminating the variables u, v, w from the ideal I as given in (8).

We begin with the elimination of the variable w. Afterward, we reduce the whole elimination process to the computation of a single resultant with respect to v.

Lemma 1. *With the previous notation let* $I = \langle F, G, 1 - w(f^2+g^2)\rangle \subset K[x,y,z,v,w]$. *Then,* $I \cap K[x,y,z,v] = \langle F, G, H\rangle$.

Proof. In order to prove the equality of the two ideals we use several facts from commutative algebra (see [14] for reference). We will use the abbreviations $S = K[x, y, z, v, w]$ and $R = K[x, y, z, v]$.

First of all note that $S/I \simeq R[1/h]/\langle F, G\rangle$, where $h = f^2 + g^2$. Therefore $I \cap R = (\langle F, G\rangle)^{\text{sat}}$, where the saturation is taken with respect to h. That is $I \cap R = \langle F, G\rangle : h^n$ for $n \gg 0$. In order to continue we prove the equality

$$\langle F, G\rangle = \langle f, g\rangle \cap J, \tag{19}$$

where $J = \langle F, G, H\rangle$. Clearly, $\langle f, g\rangle \cap J = \langle F, G, \langle f, g\rangle \cap \langle H\rangle\rangle$. But now $\{f, g\}$ forms a regular sequence since $f, g \in K[x, v]$ do not have a common factor by our general assumptions. Therefore, $\{f, g, H\}$ forms also a regular sequence and $\langle f, g\rangle : H = \langle f, g\rangle$. That implies

$$\langle F, G, \langle f, g\rangle \cap \langle H\rangle\rangle = \langle F, G, \langle f, g\rangle H\rangle. \tag{20}$$

But now $fH = Fz + G((r - v) + y) \in \langle F, G\rangle$ and $gH = Gz + F((r - v) - y) \in \langle F, H\rangle$. This finally proofs (19).

By virtue of (19) it is enough to show that the ideal $\langle F, G, H\rangle$ is saturated with respect to $h = f^2 + g^2$. That is we have to prove that $\langle F, G, H\rangle : h = \langle F, G, H\rangle$. Because H is irreducible it follows that $J = \langle F, G, H\rangle$ is an ideal with $\text{height } J \geq 2$. By the presentation of J as the determinantal ideal in Proposition 2 we get $\text{height } J \leq 2$ and therefore $\text{height } J = 2$. By the Hilbert-Burch Theorem it follows that R/J is a perfect ideal. So any associated prime ideal P of R/J is of height 2.

Now suppose there is an associated prime ideal P of R/J such that $h = f^2 + g^2 \in P$. Because of $(f^2 + g^2)z - 2(r - v)fg = Ff + Gg \in J \subseteq P$ it follows also that $2(r - v)fg \in P$. Since $r - v \notin P$ we get either $f \in P$ or $g \in P$. Because of $f^2 + g^2 \in P$ this implies in both cases $f, g \in P$. Due to $H \in J \subseteq P$ this shows that $f, g, H \in P$. Since $\{f, g, H\}$ is a regular sequence it yields that $\text{height } P \geq 3$. But this contradicts the fact that $\text{height } P = 2$ as a consequence of the unmixedness of J and $\text{height } J = 2$. Whence, there is no associated prime ideal P of R/J such that $h = f^2 + g^2 \in P$. Therefore $J : h = J$, which proves that the ideal is saturated. □

Now, we get the equation of the implicit surface of the blowup by the following corollary.

Corollary 1. *The defining equation $\mathcal{F}$ of the implicit surface of the toroidal blowup is given by the elimination ideal*

$$\langle \mathcal{F}\rangle = \langle F, G, H\rangle \cap K[x, y, z]. \tag{21}$$

Proof. By our above consideration the equation of $\mathcal{F}$ is given by the elimination of the variable v in the ideal $J \subset K[x, y, z, v]$. □

2.3 Resultants

One way to compute the elimination ideal is to use an elimination ordering and to compute the corresponding Gröbner bases (see, e.g., [5]). A much simpler method is based on resultants, which can be used to eliminate a single variable in a system of two polynomials. In this section, we will reduce the computation of $\mathcal{F}$ to the calculation of a single, rather simple resultant.

Theorem 1. *The defining equation $\mathcal{F}$ of the elimination ideal $\langle \mathcal{F}\rangle$ of $I \cap K[x, y, z]$ can be computed by*

1. $\mathcal{F} = \mathcal{F}(F, H) = \text{Res}_v(F, H)/z$,
2. $\mathcal{F} = \mathcal{F}(G, H) = \text{Res}_v(G, H)/z$.

Here, $F = fz - ((r - v) + y)g$, $G = gz - ((r - v) - y)f$, $H = y^2 + z^2 - (r - v)^2$ and $f, g \in K[x, v]$ are obtained from the original $f, g \in K[u, v]$ by substituting $u = x$.

Proof. From Corollary 1 it follows that the elimination ideal $\langle \mathcal{F}\rangle$ is given by $J \cap T$, where $J = \langle F, G, H\rangle$ and $T = K[x, y, z]$. Now, we apply Proposition 2 and obtain

$$(J \cap T) \cap (\langle (r - v) + y, z\rangle \cap T) = \langle F, H\rangle \cap T, \tag{22}$$

$$(J \cap T) \cap (\langle (r - v) - y, z\rangle \cap T) = \langle G, H\rangle \cap T. \tag{23}$$

But this implies that $\langle \mathcal{F}\rangle \cdot \langle z\rangle = \langle \text{Res}_v(F, H)\rangle$ and $\langle \mathcal{F}\rangle \cdot \langle z\rangle = \langle \text{Res}_v(G, H)\rangle$. To this end recall that $\langle (r - v) + y, z\rangle \cap T = \langle (r - v) - y, z\rangle \cap T = \langle z\rangle$. □

As a consequence of Theorem 1 we are able to compute the implicit form of the toroidal blowup just by one resultant and subsequently dividing out the variable z. Clearly, one should compute the resultant, which involves the polynomials with the lowest degree. Let us continue with a consideration of the complexity of the calculation of the resultant. In fact, it turns out that this resultant is easy to compute.

Lemma 2. *The computation of the polynomial $\mathcal{F}$ requires $\mathcal{O}(\max(\deg_v f, \deg_v g))$ operations in $K[x, y, z]$.*

Proof. We will only show the case of

$$\mathcal{F} = \text{Res}_v(F, H)/z = (-1)^{\deg F}\text{Res}_v(F, -H)/z$$

and use the notation $F = \sum_{i=0}^{d} f_i v^i$ and $-H = v^2 + -2r)v + (r^2 - y^2 - z^2)$. Let $\tilde{F} = F \bmod_v(-H)$, then

$$\text{Res}_v(F, -H) = \text{lcoeff}(-H)^{d - \deg_v \tilde{F}}\text{Res}_v(\tilde{F}, -H) \tag{24}$$

$$= \text{Res}_v(\tilde{F}, -H), \tag{25}$$

as follows from the properties of the resultant (see [15, Theorem 9.4]). Although the polynomials have their coefficients in $K[x, y, z]$, the remainder $\tilde{F}$ can be easily computed by polynomial long division with respect to v. Recall that $-H$ is a monic polynomial in the variable v. Because of $\deg H = 2$ we have $\tilde{F} = \tilde{f}_1 v + \tilde{f}_0$ with $\tilde{f}_0, \tilde{f}_1 \in K[x, y, z]$. Thus, the final result is obtained by

$$\text{Res}_v(\tilde{F}, -H) = \begin{vmatrix} \tilde{f}_1 & \tilde{f}_0 & 0 \\ 0 & \tilde{f}_1 & \tilde{f}_0 \\ 1 & -2r & r^2 - y^2 - z^2 \end{vmatrix} \tag{26}$$

$$= \tilde{f}_0^2 + 2r\tilde{f}_1\tilde{f}_0 + (r^2 - y^2 - z^2)\tilde{f}_1^2. \tag{27}$$

The number of arithmetic operations in $K[x, y, z]$ for the computation of $\tilde{F}$ is bounded by $\mathcal{O}(d)$, where $d = \max(\deg_v f, \deg_v g)$. The costs for the division $\text{Res}_v(\tilde{F}, -H)/z$ are insignificant. □

Furthermore, the proof of Lemma 2 provides an efficient, easily implementable algorithm for the computation of $\mathcal{F}$. In fact, only basic arithmetic of polynomials is necessary.

2.4 Degree Bounds

In general, the result of an implicitization has a degree that is quadratic in the degree of the underlying rational parametrization (see, e.g., [13]). Thus, even for low degree parametric surfaces the efficient visualization using the implicit form might become infeasible. In the following, we show that the degree bounds for the implicit surface of the toroidal blowup depend only linear on the degrees of $f, g \in K[u, v]$. These bounds are not only of theoretical interest. They provide significant information on the computational effort for the visualization.

Lemma 3. *The degrees of x, y and z in $\mathcal{F}$ are bounded by*

$$\deg_x \mathcal{F} \leq 2 \max(\deg_x f, \deg_x g) + 2 \tag{28}$$

$$\deg_y \mathcal{F} \leq 2 \max(\deg_v f, \deg_v g) + 4 \tag{29}$$

$$\deg_z \mathcal{F} \leq 2 \max(\deg_v f, \deg_v g) + 3. \tag{30}$$

The total degree of $\mathcal{F}$ is bounded by

$$\deg \mathcal{F} \leq 4 \max(\deg f, \deg g) + 3. \tag{31}$$

Proof. With $t \in \{x, y, z, \text{total}_{xyz}\}$ we have the following bounds on the degrees occurring in the resultant (see, e.g., [16]):

$$\begin{aligned} &\deg_t \text{Res}_v(F, H) \\ &\quad \leq \deg_t F \deg_v H + \deg_t H \deg_v F. \end{aligned} \tag{32}$$

The result is obtained by inserting the respective degrees of F and H, repeating the process with G and H, and selecting the smallest of both bounds. For the total degree and the degree in z we take into account that the resultant is divisible by z. □

These bounds show that the degree of the implicit equation of the toroidal blowup does not explode as one would expect from the original definition in (8). The key ingredient for the linear bound is the change of the generating set of polynomials from A, B, $1 - w(f^2 + g^2)$ to F, G, H, where H does not depend on f and g. Together with the reduction of the computation to a single resultant we get the linear degree bounds. As a side effect, the polynomials f and g appear only linear in F and G, while they appear with its squares in A, B, and $1 - w(f^2 + g^2)$. This allows to reduce the degree bound by another constant factor.

Remark 1. The actual total degree of the examples that we consider in Section 4 is even much lower than the worst case bound we obtained in Lemma 3. According to our experiments, the total degree usually does not exceed the degree with respect to the individual variables. However, it might by possible to construct polynomials that hit the degree bound.

2.5 Deformations

A main motivation for our work is the visualization of deformations of blowups, i.e., the case where f and g depend on a certain number of parameters $a_i \in K$. By an interactive visualization it is possible to study the deformation of the surface when the a_i vary. This approach will be helpful for the deformations we have in mind as explained above.

In general, the specialization of parameters and the computation of resultants cannot be interchanged. To perform an efficient visualization, we need to ensure that we can compute $\mathcal{F} \in K[x, y, z, a_1, \ldots, a_l]$ symbolically and then specialize the parameters in every frame of the deformation. The following result gives a description of the behavior of the specialized implicit surface of the toroidal blowup.

Lemma 4. *Let φ be a homomorphism from $K[x, y, z, a_1, \ldots, a_l]$ to a subring obtained by a specialization of a subset of the variables $a_1, \ldots, a_l$ to elements in K such that $V(\varphi(f), \varphi(g))$ consists of a finite number of points. Then,*

$$\varphi(\mathcal{F}(F, H)) = \pm \mathcal{F}(\varphi(F), \varphi(H)), \tag{33}$$

$$\varphi(\mathcal{F}(G, H)) = \pm \mathcal{F}(\varphi(G), \varphi(H)). \tag{34}$$

Proof. Under the specialization φ the v-degree of the polynomials f, g could change. This is propagated to F and G. In order to check what happens with $\mathcal{F}$ we apply the specialization property of resultants (see [16], [15]): If $\deg_v \varphi(F) = \deg_v F - k$ and $\deg_v \varphi(H) = \deg_v H$, then

$$\varphi(\text{Res}_v(F, H)) = \varphi(\text{lcoeff}_v(H))^k \text{Res}_v(\varphi(F), \varphi(H)). \tag{35}$$

The condition $\deg_v \varphi(H) = \deg_v H$ is always satisfied, since $-H$ is a monic polynomial with respect to v. Hence, this allows us to simplify the previous formula to

$$\varphi(\text{Res}_v(F, H)) = \pm \text{Res}_v(\varphi(F), \varphi(H)), \tag{36}$$

and therefore

$$z\varphi(\mathcal{F}(F, H)) = \varphi(z\mathcal{F}(F, H)) \tag{37}$$

$$= \pm z\mathcal{F}(\varphi(F), \varphi(H))). \tag{38}$$

The same arguments hold if $\mathcal{F}$ is computed using G and H. □

When additional parameters are introduced, $\mathcal{F}$ will usually contain a lot more terms. However, this does not add much overhead to the visualization, since the a_i might be specialized prior to the rendering process. Due to Lemma 4 $\varphi(\mathcal{F}(F, H))$ has the same number of terms as $\mathcal{F}(\varphi(F), \varphi(H))$. Examples of deformations of blowups and their visualization are shown in Figs. 8 and 9.

2.6 The Degeneration

The assumption of $\dim(V(\varphi(f), \varphi(g))) = 0$ in Lemma 4 is fulfilled for parameters of an open subset of K^l. A degeneration occurs whenever $\dim V(\varphi(f), \varphi(g))$ becomes positive. We will now discuss these degenerations. For simplicity let us denote the specialized $\varphi(f), \varphi(g)$ again by f, g. Then, algebraically the degeneration means that $f = h \cdot \tilde{f}, g = h \cdot \tilde{g}$ for a nonconstant polynomial $h \in K[u, v]$ and relatively prime polynomials $\tilde{f}, \tilde{g}$. Therefore, $\tilde{X} = V(\tilde{f}, \tilde{g})$ consists of a finite number of points in $\mathbb{A}^2_K$.

In our elimination process, we have to compute the resultant $\text{Res}_v(F, H)$ resp. $\text{Res}_v(G, H)$. In this discussion, we restrict ourselves to the first resultant. Define $\tilde{F} = \tilde{f}z - ((r - v) + y)\tilde{g}$. Then the definition of the resultant as the product of the pairwise differences of roots (see, e.g., [15, Theorem 9.3 (i)]) provides the equality

$$\mathrm{Res}_v(F,H) = \mathrm{Res}_v(h,H)\cdot \mathrm{Res}_v(\tilde{F},H). \tag{39}$$

The surface $\tilde{\mathcal{F}}$ of the toroidal blowup of $V(\tilde{f},\tilde{g})$ is obtained by dividing the resultant $\mathrm{Res}_v(\tilde{F},H)$ by z. Thus, the surface $\mathcal{F}$ of the blowup of the degenerated set $X = V(f,g)$ is

$$\mathcal{F} = \mathcal{H}\cdot\tilde{\mathcal{F}}, \tag{40}$$

where $\mathcal{H} = \mathrm{Res}_v(h,H)$. Let $(u_0,v_0)\in\mathbb{D}$ such that $h(u_0, v_0) = 0$. Then, a point (x_0,y_0,z_0) with $x_0 = u_0$ satisfies $H(x_0,y_0,z_0) = 0$ if and only if $v = v_0$. That is, H vanishes on the whole circle $y^2+z^2 = (r-v_0)^2$ of the plane $x = x_0 = u_0$. In other words, $\mathcal{H}$ is the image of the cylinder over $h = 0$ mapped to the torus by the toroidal embedding. Hence, the surface $\mathcal{F}$ is the union of the toroidal blowup of $V(\tilde{f},\tilde{g})$ and $\mathcal{H}$. For an example with $V(\tilde{f},\tilde{g}) = \emptyset$ we refer to Fig. 10a.

3 Visualization of the Implicit Form

During the derivation of the results of the previous section, we used the abstract field K. In order to visualize toroidal blowups we set $K = \mathbb{R}$ again for the remaining part of the paper. Thus, the toroidal blowups are now defined in three-dimensional affine space. We will use $V(\mathcal{F}) = V_{\mathbb{R}}(\mathcal{F})$ for the real zero-set of $\mathcal{F}$. A point $P\in V(\mathcal{F})$ of the implicit form of the parametric surface $P(u,v)$ might originate from complex, not necessarily real, parameter values $(u,v)\in\mathbb{C}^2$. Fortunately, this is not the case for toroidal blowups.

Proposition 3. *Let $P(u,v)\in V_{\mathbb{R}}(\mathcal{F})$, then $(u,v)\in\mathbb{R}^2$.*

Proof. For a given point $P\in V_{\mathbb{R}}(\mathcal{F})$ of the implicitly given surface we use (3) for the computation of the parameters u and v such that $P = (x(u,v),y(u,v),z(u,v))$. Therefore,

$$y(u,v)^2 + z(u,v)^2 = (v-r)^2(\cos^2\alpha+\sin^2\alpha) \tag{41}$$

$$= (v-r)^2, \tag{42}$$

and we have

$$u = x,\ v = r\pm\sqrt{y^2+z^2}. \tag{43}$$

Since $x,y,z,r\in\mathbb{R}$, the parameters u and v have to be real valued, too. □

Given this result, we proceed with the visualization. Implicitly defined surfaces can either be converted into a polygon mesh for rendering or they can be rendered directly using ray tracing techniques. The latter ones usually provide an excellent quality of the visualization. Although ray tracing is often considered to be computationally intense, recent advances in graphics hardware technology permit the interactive display of algebraic surfaces (provided the degree is not too large) by a simplified method called ray casting.

In the ray casting algorithm, the geometry visible to the viewer is computed by intersecting rays with the objects in the scene. Basically, at least one ray from the virtual eye point through each pixel of the image plane is considered. In order to find the intersection points of an algebraic surface $\mathcal{F}(x,y,z) = 0$ and the ray $r(t) = (x(t),y(t),z(t))$, the univariate polynomial equation $\mathcal{F}(x(t),y(t),z(t)) = 0$ has to be solved, using, e.g., numerical real root finders. Then, the set of intersection points is clipped to a predefined bounding geometry, which is a torus in our case. More sophisticated clipping techniques might be applied (see Section 3.1). The remaining points are textured and illuminated using some light reflection model and the computed color is assigned to the corresponding pixel. We skip further details for brevity and refer to standard literature on computer graphics, e.g., [17].

The above algorithm has been adjusted to fit the requirements for an implementation on graphics processors. This has been demonstrated in [8], [7], [9], [10], [11] and others. Therefore, we will only discuss our contributions and omit the details that have been covered in the existing literature.

3.1 Clipping $V(\mathcal{F})$ to $\mathbb{T}_{f,g}$

In general, the surface $V(\mathcal{F})$ is unbounded and contains much more geometry, than we actually want to visualize. Because of $\mathbb{T}_{f,g}\subseteq V(\mathcal{F})$, we have to eliminate $V(\mathcal{F})\setminus\mathbb{T}_{f,g}$ for the visualization. In principle, the parametric form $P(u,v)$ allows the computation of most of the points of $\mathbb{T}_{f,g}$ by the restriction of (u,v) to $\mathbb{D}$. In the implicit form this correspondence is lost and has to be reconstructed. To be more precise, for a given point $P\in V(\mathcal{F})$ we have to decide whether there exists an $(u,v)\in\mathbb{D}\setminus V(f,g)$, such that $P = (x(u,v),y(u,v),z(u,v))$, or whether P is located on the exceptional fiber.

To cut off the surface geometry that is outside the $\mathbb{D}$-torus we have two simple possibilities. The first one is to clip each ray against the $\mathbb{D}$-torus, which results in zero, one or two search intervals for the numerical real root finder. The second possibility is to compute all intersections of the ray and the blowup. Then, one checks for each intersection point if it is inside the $\mathbb{D}$-torus. The latter test can be performed in an easy way by checking whether one of the solutions of (43) is contained in $\mathbb{D}$. Fig. 5 illustrates which geometry is cut off.

By definition, all points $P(u,v)$ with $(u,v)\in\mathbb{D}\setminus V(f,g)$ are contained within the $\mathbb{D}$-torus. However, the converse is not true. Thus, the visualization of the implicit form of the blowup inside the $\mathbb{D}$-torus often shows points $P(u,v)$ with $(u,v)\notin\mathbb{D}$. Fig. 5b illustrates this problem for the case of a simple surface.

For a point inside the $\mathbb{D}$-torus we always have a solution $(u_0,v_0)\in\mathbb{D}$ and a solution $(u_1,v_1)\notin\mathbb{D}$ (remember that $r>\rho$). The three points P, $P_0 = P(u_0,v_0)$ and $P_1 = P(u_1,v_1)$ are located on a circle with radius $|r-v|$ in the plane $x = u$. A small angle between the position vectors of P and P_0 suggests $P = P_0\in\mathbb{T}_{f,g}$.

As we have seen in Section 1.3, the evaluation of P_0 is likely to be numerically very unstable due to the common zeros of f and g in $\mathbb{D}$. Moreover, $P(u_0,v_0)$ is not even defined for $(u_0,v_0)\in V(f,g)$. The error that is introduced in the visualization by using the above criterion to clip the surface is shown in Fig. 6.

To overcome this difficulty we investigate the solution (u_1,v_1) instead of (u_0,v_0). We are interested in visualizing the blowup surface for some points in $\mathbb{D}$ and given f and g such that all their common zeros are contained in $\mathbb{D}$. Due to $(u_1,v_1)\notin\mathbb{D}$ the evaluation of $P(u_1,v_1)$ is in most cases well-conditioned. Note that the denominator $f(u_1,v_1)^2+g(u_1,v_1)^2$ is always nonzero and bounded. Now, we draw P provided

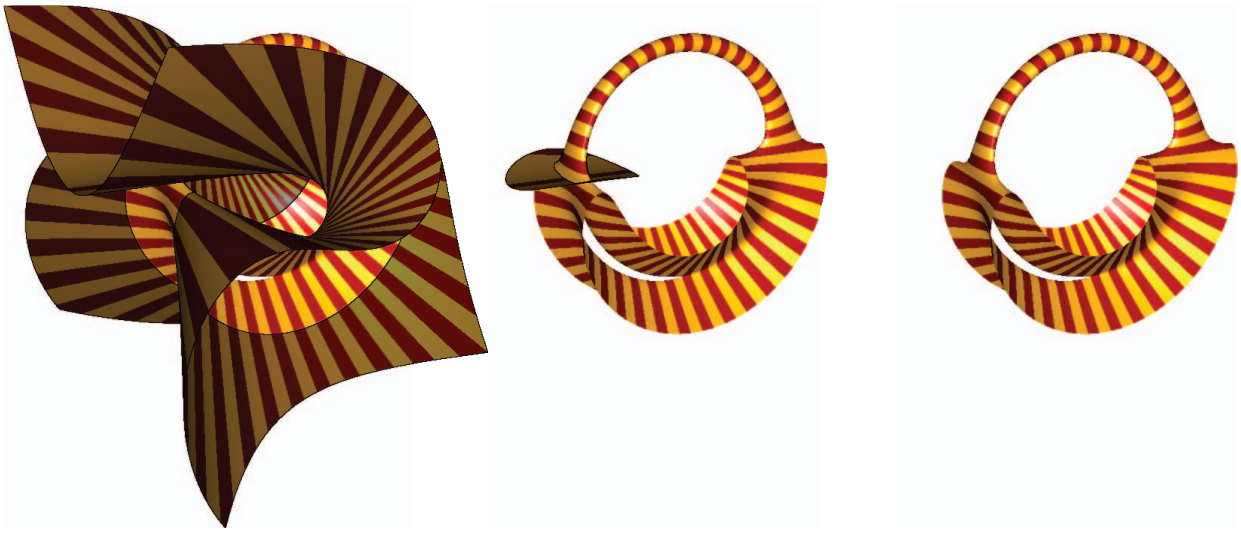

(a) No clipping. (b) Clipping against the $\mathbb{D}$-torus. (c) Clipping to the set $\mathbb{T}_{f,g}$.

Fig. 5. (a) This part shows the surface of $\mathcal{F}$ without clipping against the $\mathbb{D}$-torus. The surface is unbounded and only clipped to a box for the illustration. The surface parts with dark painting are outside the $\mathbb{D}$-torus. (b) This part shows the inside part. The dark painted part of (b) results from the second solution in (43). It does not belong to the toroidal blowup, since $(u_1, v_1) \notin \mathbb{D}$. (c) This part shows the final result.

Fig. 6. Rendering artifacts caused by the naïve idea of clipping $V(\mathcal{F})$ to $\mathbb{T}_{f,g}$: $P \in V(\mathcal{F})$ either corresponds to $P_0 = P(u_0, v_0)$ for $(u_0, v_0) \in \mathbb{D}$ or to $P_1 = P(u_1, v_1)$ for $(u_1, v_1) \notin \mathbb{D}$. P should be displayed if $P = P_0$, i.e., corresponds to a point above the disc, and discarded otherwise. The evaluation of $P_0 = P(u_0, v_0)$ using the parametric form is numerically very unstable. Therefore, many points close to the exceptional circles are accidentally clipped. This does not happen, if (44) is used for the clipping instead (see, e.g., Fig. 5c), which is based on the evaluation of $P_1 = P(u_1, v_1)$.

$$\measuredangle(\vec{P}, \vec{P}_1) > \varepsilon_1. \tag{44}$$

The motivation for this test is as follows: If $(u_1, v_1) \neq (u_0, v_0)$, the point $P(u_1, v_1)$ is not in $\mathbb{T}_{f,g}$. If the angle between $P(u_1, v_1)$ and P is nonzero or (in the case of round-off error) larger than a predefined ε_1, then P is considered to be in $\mathbb{T}_{f,g}$ and therefore will be visualized.

In the implementation of our test the angle is not computed directly. Instead we use its sine and cosine, which are easy to determine by appropriate projections. After some simplifications and with $(f_i, g_i) = (f(u_i, v_i), g(u_i, v_i)), i = 0, 1$, we get

$$\sin\measuredangle(\vec{P}, \vec{P}_1) = \frac{\vec{P}^{\perp} \cdot \vec{P}_1}{\|\vec{P}^{\perp}\| \cdot \|\vec{P}_1\|} \tag{45}$$

$$= \operatorname{sgn}(r - v_1) \frac{(-P_z, P_y) \cdot \left(f_1^2 - g_1^2, 2 f_1 g_1\right)}{|r - v_0|\left(f_1^2 + g_1^2\right)}, \tag{46}$$

$$\cos\measuredangle\left(\vec{P}, \vec{P}_1\right) = \frac{\vec{P} \cdot \vec{P}_1}{\|\vec{P}\| \cdot \|\vec{P}_1\|} \tag{47}$$

$$= \operatorname{sgn}(r - v_1) \frac{(P_y, P_z) \cdot \left(f_1^2 - g_1^2, 2 f_1 g_1\right)}{|r - v_0|\left(f_1^2 + g_1^2\right)}. \tag{48}$$

For small angles, a linear function is a good approximation of the sine. The cosine is only needed to decide whether $\measuredangle(\vec{P}, \vec{P}_1) \approx 0$ or $\measuredangle(\vec{P}, \vec{P}_1) \approx \pm\pi$. Therefore, (44) transforms into the condition

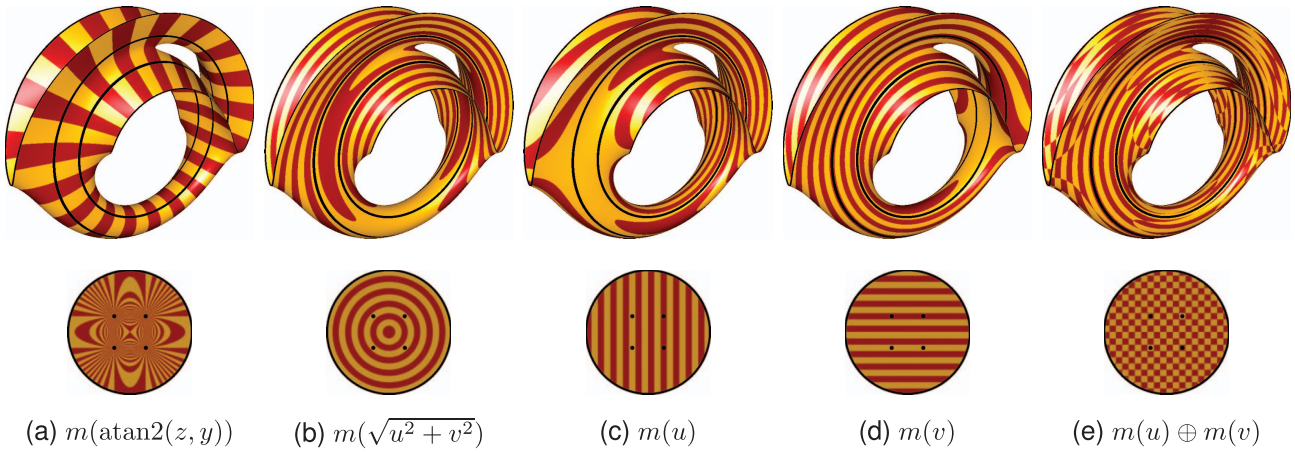

Fig. 7. Some texturing patterns of blowup surfaces and the underlying disc $\mathbb{D}$ using (53). The function $m(\cdot)$ computes a Boolean value, that is used to choose either the red or the yellow material. In (a) the texturing of a point is derived from its position in the $\mathbb{D}$-torus. In the other examples the surface is textured by some texturing of the disc $\mathbb{D}$ according to the (u,v) coordinates. The black color illustrates $V(f,g)$ and the boundary of the disc $\mathbb{D}$ and how both are projected onto the toroidal blowup. That is, the black coloured circles in the toroidal blowups visualize the exceptional fibers.

$$|\sin \measuredangle(\vec{P},\vec{P}_1)| > \varepsilon_1 \wedge \cos \measuredangle(\vec{P},\vec{P}_1) \geq 0, \tag{C1}$$

for the acceptance of P as a valid solution.

This test works well as long as P_0 and P_1 are far apart. But it will fail, e.g., at self-intersections of the surface, so that more geometry is clipped than actually necessary. This results in small gaps in the visualization. In order to improve the image quality we resolve this by accepting a point P that does not pass the test (C1), but satisfies $\measuredangle(\vec{P}_0,\vec{P}_1) < \varepsilon_2$. With the above notation we have

$$\sin \measuredangle(\vec{P}_0,\vec{P}_1) = \frac{\vec{P}_0^{\perp} \cdot \vec{P}_1}{\|\vec{P}_0^{\perp}\| \cdot \|\vec{P}_1\|} \tag{49}$$

$$= -\frac{(2f_0g_0, g_0^2 - f_0^2) \cdot (f_1^2 - g_1^2, 2f_1g_1)}{(f_0^2+g_0^2)(f_1^2+g_1^2)}, \tag{50}$$

$$\cos \measuredangle(\vec{P}_0,\vec{P}_1) = \frac{\vec{P}_0 \cdot \vec{P}_1}{\|\vec{P}_0\| \cdot \|\vec{P}_1\|} \tag{51}$$

$$= -\frac{(f_0^2 - g_0^2, 2f_0g_0) \cdot (f_1^2 - g_1^2, 2f_1g_1)}{(f_0^2+g_0^2)(f_1^2+g_1^2)}. \tag{52}$$

So, a previously discarded point P is visualized, provided

$$|\sin \measuredangle(\vec{P}_0,\vec{P}_1)| < \varepsilon_2 \wedge \cos \measuredangle(\vec{P}_0,\vec{P}_1) \geq 0. \tag{C2}$$

In order to close the gap at a self-intersection that is caused by the angle ε_1 in (C1) completely the error bound ε_2 is chosen to be slightly larger than ε_1. The results of the combined tests are shown in Fig. 5c. In this example, the clipping is performed correctly at all pixels of the image.

Remark 2. Note that only the sign of the cosine is used in both tests. Therefore, the divisions in (48) and (52) are unnecessary and might be skipped. In addition, it is important to mention that the test (C2) needs an expression similar to those for the computation of $P(u_0,v_0)$, which one should avoid due to the numerical instabilities. Nevertheless, in this test the instability is only significant for the small number of points that are close to the exceptional fiber and additionally close to a self intersection. Therefore, notable clipping errors are rare in practice.

3.2 Texturing the Surface

The texture of the surface should be chosen to enable a viewer to obtain additional information about the blowup or to understand its structure more easily. Two types of coloring schemes seem to be useful: Either the texture of a point is chosen with respect to its (x,y,z)-coordinates or with respect to its (u,v)-coordinates. For each point $P \in \mathbb{T}_{f,g}$ the material is computed using

$$m(d) = \begin{cases} true & (s \cdot d \bmod 2) > 1, \\ false & \text{otherwise}, \end{cases} \tag{53}$$

where d is a measure based on either the (x,y,z)- or (u,v)-coordinates of P, s is some user defined factor to scale the pattern, mod is the floating point modulus, and the Boolean values are interpreted as two different materials. A few examples of texturing schemes utilizing $m(\cdot)$ are illustrated in Fig. 7 for the blowup of $X = \{\pm 1, \pm 1\}$ as the zero set $V(f,g)$ with $f = u^2 - 1, g = v^2 - 1$.

In Fig. 7a, the parameter d of a point P is based on the angle between $\vec{P}$ and the y-axis. Mapping the resulting coloring scheme to the disc $\mathbb{D}$ produces the contour lines of $z = f(u,v)/g(u,v)$, i.e., of the nontoroidal blowup of the disc.

The other texturing schemes in Fig. 7 compute d using the (u,v) coordinates of P. Thus, actually the disc $\mathbb{D}$ is textured. Mapping this texture onto the surface shows how different subdivision schemes of the parameter domain (u,v) would affect a triangulation of the surface that is obtained from the parametric form. The problems of a uniform subdivision of the (u,v)-domain (mentioned in Section 1.3) become clear in Fig. 7e since the checkerboard pattern is heavily stretched in the toroidal blowup.

3.3 Highlighting the Exceptional Fibers

While all points $\mathbb{D} \setminus V(f,g)$ are mapped to a single point in the $\mathbb{D}$-torus, the points $X = V(f,g)$ appear as circles in the toroidal blowup. In order to visualize these circles on the surface, it is not sufficient to test $|f(u,v)| \leq \varepsilon$ and $|g(u,v)| \leq \varepsilon$. This leads to circles of nonconstant width in the visualization.

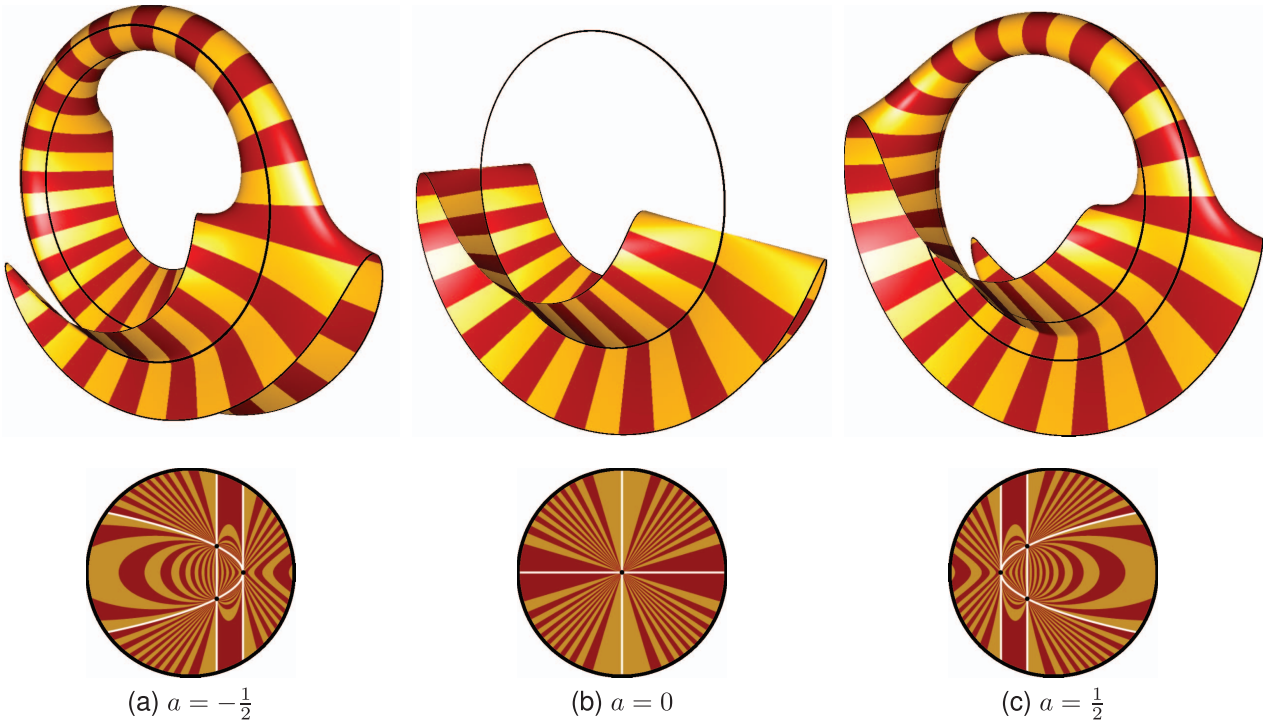

Fig. 8. Visualization of the toroidal blowup of three dynamic points with $f(u,v) = au + v^2 - 2a^2$, $g(u,v) = (u-2a)(u-a)$, $r = 4$, and $\rho = 2$. For $a = 0$ the double point and the two simple points collapse into a fourfold point. The surface $\mathcal{F}$ is of total degree 5 and is rendered with approximately 125 frames per second.

A more appropriate choice is to use the (u,v) coordinates of the exceptional points directly. For many interesting examples (including those shown in this paper), the set of exceptional points $X = V(f,g)$ is known a priori or can be computed easily. Thus, we can either render a torus of small width over each exceptional point or draw points from $\mathbb{T}_{f,g}$ with similar (u,v) coordinates in a different color. This first approach is used in Fig. 8b. Examples of the latter technique are shown in Figs. 7, 9, and 10.

4 Implementation and Results

In the previous sections, we described an efficient way to find the implicit equation of the parametric form of a toroidal blowup. We discussed a ray tracing technique for its visualization as well as several clipping methods in order to get the correct visualization of the toroidal blowup over a disc $\mathbb{D}$ as suggested by Brodmann in [4]. In addition, we included the visualization of the exceptional fiber. Also, we investigated approaches on how to avoid artifacts that might occur in particular visualizations. In this section, we want to discuss an implementation of a renderer. We do this by several examples illustrating the difficulties that might occur.

4.1 Real Surf as a Tool for Toroidal Blowups

The program REALSURF (see [8], [7], [9]) was designed for the interactive visualization of implicit surfaces in real time. It supports additional parameters for an interactive deformation of the given surface. Using this tool, the ray tracing and clipping routines are processed directly on the graphics processing unit of the graphics card. In our case, this is a NVIDIA GEFORCE GTX 460. With an additional script that implements the newly introduced clipping and texturing and the highlighting of the exceptional fiber, REALSURF is used for all ray casting-based renderings of toroidal blowups in this paper. The visualization is performed in real time for all of them.

It is worth to mention that the current prototypical implementation of the rendering algorithm is efficient for surfaces that have a compact representation with few terms. Our equations for the toroidal blowups are in monomial form and hence contain a lot of terms. First experiments suggest that for the examples considered here, the speed of the visualization might be increased by a factor of 5 to 10 by taking advantage of appropriate data structures for polynomials with dense coefficient arrays.

4.2 Discussion of Examples

We will now continue by presenting some practical results. In the figures, the texturing is performed according to Fig. 7a. Therefore, the coloring of the disc $\mathbb{D}$ corresponds to contour lines of $z = f/g$. The sets $V(f)$ and $V(g)$ are illustrated in $\mathbb{D}$ using white color, while $X = V(f,g)$ is marked using black dots. Refresh rates for the interactive rendering at a display size of 512×512 are listed in the captions of the figures.

4.2.1 Deformation of Points

In Fig. 8, the common zero-set of $f = au + v^2 - 2a^2, g = (u-2a)(u-a)$ is deformed by the parameter $a \in \mathbb{R}$. We get two simple points $(a, \pm a)$ and a double point $(2a, 0)$ on a parabola for $a \neq 0$. The construction is symmetric for $+a$ and $-a$. The three points collapse into a fourfold point for $a = 0$ in the origin. This surface is known as Whitney's double umbrella (topologically equivalent to Plücker's conoid).

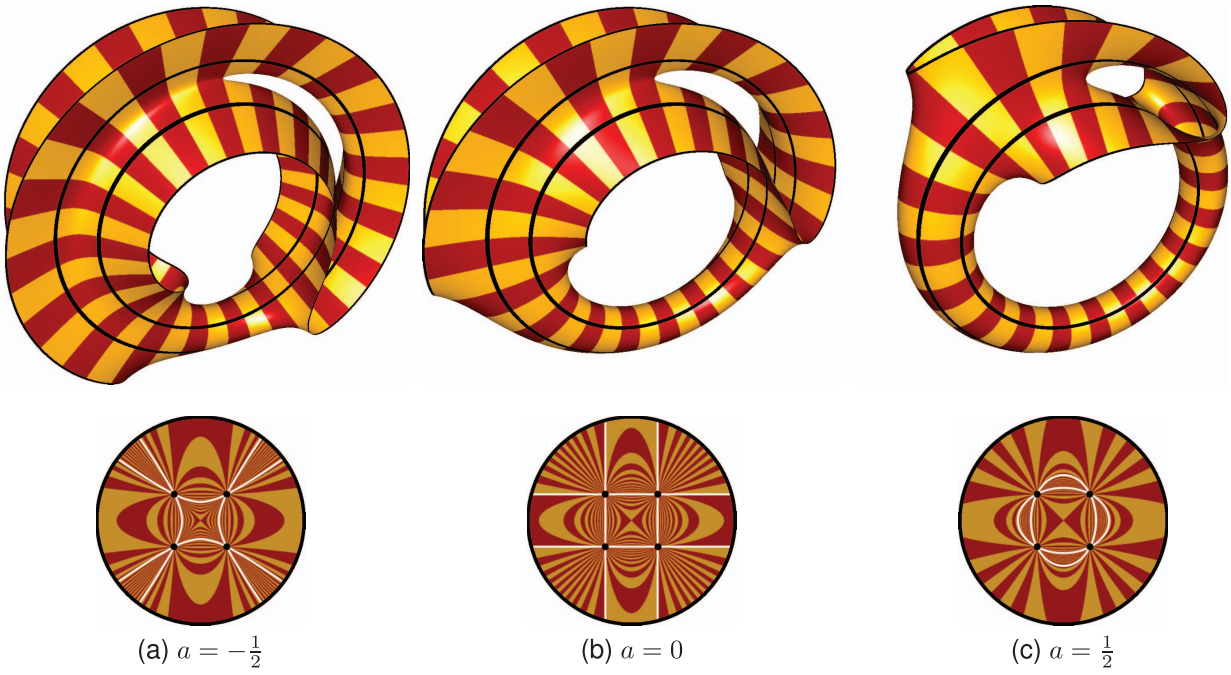

(a) $a = -\frac{1}{2}$ (b) $a = 0$ (c) $a = \frac{1}{2}$

Fig. 9. Visualization of the toroidal blowup of four static points with $f(u,v) = u^2 + av^2 - a - 1$, $g(u,v) = au^2 + v^2 - a - 1$, $r = 8$, and $\rho = 4$. The equation of the surface is of total degree 7 and is rendered with approximately 80 frames per second.

(a) A degeneration of the example in Figure 9 with $a = 1$. $\deg(\mathcal{F}) = 7$; 80 fps.

(b) Elliptic curve intersecting a double line. $\deg(\mathcal{F}) = 7$; 55 fps.

(c) "The Algebraic Wizard Hat". $\deg(\mathcal{F}) = 9$; 12 fps.

(d) Blowup of five points in the plane. $\deg(\mathcal{F}) = 7$; 36 fps.

Fig. 10. Some more examples of blowups.

4.2.2 Deformation of Defining Equations

In Fig. 9, the deformed polynomials $f = u^2 + av^2 - a - 1$ and $g = au^2 + v^2 - a - 1$ always intersect in the same set of points $\{\pm 1, \pm 1\}$ provided that $a \in \mathbb{R} \setminus \{\pm 1\}$. If $a < 0$, then $V(f)$ and $V(g)$ are hyperbolas, while they are ellipses for $a > 0$. Both yield two parallel lines for $a = 0$. Note that Fig. 9b (i.e., $a = 0$) shows the computer generated image of the toroidal blowup of 4 points of the plane included as a hand drawing in [4].

4.2.3 A Degeneration

Using the values $a = \pm 1$ in the previous example gives the degenerate case $\dim(V(f,g)) > 0$ mentioned in Section 2.6. Fig. 10a shows the rendering for $a = 1$ such that $f(u,v) = g(u,v) = u^2 + v^2 - 2$. Due to Section 2.6 the degeneration yields the plane $y = 0$ and the torus with tube radius $\sqrt{2}$ and central radius 8. For $a = -1$ the set $V(f,g)$ consists of the union of the two lines $u + v$ and $u - v$ intersecting in the origin.

4.2.4 Double Line and Elliptic Curve

Fig. 10b shows a toroidal blowup based on the intersection of a double line $g = v^2$ and an elliptic curve $f = v^2 - u(u-a)(u-b)$. The configuration allows deformations by two parameters. In general, $X = V(f,g)$ consists of three double points. In the case of $a = b \neq 0$, the curve f degenerates to a nodal cubic and X consists of one double and a fourfold point. For $a = b = 0$ it becomes a cuspidal cubic and X consists of a sixfold point at the origin. It is remarkable to see the detailed display of the singularities of the toroidal blowup.

4.2.5 The Algebraic Wizard Hat

The amusing surface in Fig. 10c, that we called "The Algebraic Wizard Hat," was found by accident when experimenting with the toroidal blowup based on the Chmutov Curve $f = T_4(u) + T_4(v)$ with the Chebyshev polynomial of the first kind $T_4(x) = 8x^4 - 8x^2 + 1$ of degree 4 and a circle $g = u^2 + v^2 - a^2$. The circle is chosen with a large radius a not intersecting the Chmutov Curve. Hence, the surface contains no exceptional fiber and does not span across the whole torus. Further amazing surfaces might be created by this approach.

4.2.6 Blowup in Five Points

The surface in Fig. 10d shows the toroidal blowup of the plane in five points $X = V(f,g)$ with $f = u^2 - v - 1, g = u(u-v)(u+v)$. The clipping still works well for this complex example, but the numerical real root finder in the underlying ray-casting algorithm fails for a few pixels close to the self-intersection of $V(\mathcal{F})$ on the right side of the picture.

5 Conclusion and Perspectives

The combination of our low-degree implicit form of the toroidal blowup and its interactive visualization using GPU programming yields a significant improvement compared to previous approaches. We are not only able to produce computer generated images of the hand drawn pictures of Brodmann (see [4, Figs. 10 and 11]), but also interactively visualize toroidal blowups of the disc $\mathbb{D}$ given by arbitrary coprime polynomials $f, g \in \mathbb{R}[u,v]$. The method allows interactive deformations of a set of given points as well as the deformation of the defining equations $f, g \in \mathbb{R}[u,v]$ for a fixed set X of finite points such that $X = V(f,g)$. Furthermore, texturing patterns are easily applied on a per-pixel basis. This gives a better insight into the relation between the disc $\mathbb{D}$ and the toroidal blowup $\mathbb{T}_{f,g}$.

For further investigations it would be interesting to visualize the toroidal blowup of a given plane curve C whose singularities are contained in $V(f,g)$ (see, e.g., $C_{\mathbb{T}_{f,g}}$ in Fig. 1). In order to give a better understanding of the geometry of the blowup, f and g might be highlighted on $\mathbb{T}_{f,g}$. Both problems do not seem to be easily solvable, if the curves are required to be drawn with constant width on the toroidal blowup.

Acknowledgments

The authors would like to thank Prof. M. Brodmann, who pointed us toward the problem of visualizing blowups of the plane in several points, and A. Prager, who illustrated the various drawbacks of triangle mesh-based visualizations for these type of surfaces during his diploma thesis. The authors are very grateful to the reviewers for the careful reading of the manuscript. Their comments and suggestions led to some essential improvements of the text.

References

[1] H. Hironaka, "Resolution of Singularities of an Algebraic Variety over a Field of Characteristic Zero: I & II," *The Annals of Math.*, vol. 79, pp. 109-203, 205-326, http://www.jstor.org/stable/1970486, 1964.

[2] J. Harris, *Algebraic Geometry*, Graduate Texts in Mathematics, third ed. Springer- Verlag, 1983.

[3] M. Brodmann, "Blowing-up!" *The KIAS Newsletter (English Version)*, http://www.kias.re.kr/file/NewsletterEnglish.pdf, vol. 1, pp. 40-43, 2008.

[4] M. Brodmann, "Computer-Pictures of Blowing-Ups. (Computerbilder von Aufblasungen.)," *Elementary Math.*, vol. 50, no. 4, pp. 149-163, 1995.

[5] D. Cox, J. Little, and D. O'Shea, *Ideals, Varieties, and Algorithms. An Introduction to Computational Algebraic Geometry and Commutative Algebra*, Undergraduate Texts in Mathematics, third ed. Springer, 2007.

[6] A. Prager, "Visualisierung von Mehrpunkt-Aufblasungen affiner Varietäten," master's thesis, Institut für Informatik, Martin-Luther-Universität Halle-Wittenberg, 2011.

[7] C. Stussak, "RealSurf - A GPU-Based Realtime Ray Caster for Algebraic Surfaces (Poster)," *Proc. Spring Conf. Computer Graphics*. http://realsurf.informatik.uni-halle.de, 2009.

[8] C. Stussak, "Echtzeit-Raytracing Algebraischer Flächen Auf Der Graphics Processing Unit," master's thesis, Inst. of Computer Science, Martin Luther Univ., Halle-Wittenberg, July 2007.

[9] C. Stussak and P. Schenzel, "Interactive Visualisation of Algebraic Surfaces as a Tool for Shape Creation," *Int'l J. Arts and Technology*, vol. 4, no. 2, pp. 216-228, 2011.

[10] M. Reimers and J. Seland, "Ray Casting Algebraic Surfaces Using the Frustum Form," *Computer Graphics Forum*, vol. 27, no. 2, pp. 361-370, 2008.

[11] A. Knoll, Y. Hijazi, A. Kensler, M. Schott, C. Hansen, and H. Hagen, "Fast Ray Tracing of Arbitrary Implicit Surfaces with Interval and Affine Arithmetic," *Computer Graphics Forum*, vol. 28, no. 1, pp. 26-40, http://dx.doi.org/10.1111/j.1467-8659.2008.01189.x, 2009.

[12] D. Manocha and J.F. Canny, "Implicit Representation of Rational Parametric Surfaces," *J. Symbolic Computation*, vol. 13, pp. 485-510, 1992.

[13] T.W. Sederberg and D.C. Anderson, "Implicit Representation of Parametric Curves and Surfaces," *Computer Vision, Graphics and Image Processing*, vol. 28, pp. 72-84, 1984.

[14] W. Bruns and J. Herzog, *Cohen-Macaulay Rings*, Cambridge Studies in Advanced Mathematics, Rev. ed. Cambridge Univ. Press, 1998.

[15] K.O. Geddes, S.R. Czapor, and G. Labahn, *Algorithms for Computer Algebra*. Kluwer Academic Publishers Group, 1992.

[16] F. Winkler, *Polynomial Algorithms in Computer Algebra*, Texts and Monographs in Symbolic Computation. Springer, 1996.

[17] F.S. Hill, *Computer Graphics Using OpenGL*, second ed. Prentice Hall, Inc., 2001.

Peter Schenzel received the mathematics degree at the Martin Luther University Halle-Wittenberg, the PhD degree in 1976, and the Habilitation degree in 1979. Since 1995 he has been the head of the working group for computer graphics at the Institute of Computer Science at the Martin Luther University in Halle, Germany. He got positions at the University in Paderborn, the University of Osnabrück and the Max-Planck Institute of Mathematics. His main research is related to commutative algebra and algebraic geometry. He is the author of more than 70 research articles and presented his research results as an invited speaker at several conferences.

Christian Stussak received the Diploma in computer science in 2007 from the Martin Luther University Halle-Wittenberg, where he is currently working toward the PhD degree in the field of computer graphics. As a side project he works for exhibitions presenting mathematical art. His research interests include the visualization of implicitly defined surfaces, fast and exact computer algebra, and real-time graphical effects.